

MULTILEVEL HIERARCHICAL DECOMPOSITION OF FINITE ELEMENT WHITE NOISE WITH APPLICATION TO MULTILEVEL MARKOV CHAIN MONTE CARLO

HILLARY R. FAIRBANKS¹ AND UMBERTO VILLA² AND PANAYOT S. VASSILEVSKI^{1,3}

¹*Center for Applied Scientific Computing, Lawrence Livermore National Laboratory, Livermore, CA, USA*

²*Electrical & Systems Engineering Department, Washington University in St. Louis, St. Louis, MO, USA*

³*Fariborz Maseeh Department of Mathematics and Statistics, Portland State University, Portland, OR, USA*

ABSTRACT. In this work we develop a new hierarchical multilevel approach to generate Gaussian random field realizations in a scalable manner that is well-suited to incorporate into multilevel Markov chain Monte Carlo (MCMC) algorithms. This approach builds off of other partial differential equation (PDE) approaches for generating Gaussian random field realizations; in particular, a single field realization may be formed by solving a reaction-diffusion PDE with a spatial white noise source function as the righthand side. While these approaches have been explored to accelerate forward uncertainty quantification tasks, e.g. multilevel Monte Carlo, the previous constructions are not directly applicable to multilevel MCMC frameworks which build fine scale random fields in a hierarchical fashion from coarse scale random fields. Our new hierarchical multilevel method relies on a hierarchical decomposition of the white noise source function in L^2 which allows us to form Gaussian random field realizations across multiple levels of discretization in a way that fits into multilevel MCMC algorithmic frameworks. After presenting our main theoretical results and numerical scaling results to showcase the utility of this new hierarchical PDE method for generating Gaussian random field realizations, this method is tested on a three-level MCMC algorithm to explore its feasibility.

Keywords. Gaussian random field, nonlinear Bayesian inference, Markov chain Monte Carlo, multilevel Markov chain Monte Carlo, high-dimensional uncertainty quantification, algebraic multigrid

1. INTRODUCTION

Spatially correlated random fields are commonly used in the numerical simulation of partial differential equations (PDEs) with variable coefficients. In the case where these coefficients are not well known, as is typically the case in many geophysics applications where the coefficient describes a physical parameter, the coefficient is modeled as a random field, and uncertainty quantification (UQ) may be applied as a tool to assess the reliability of the

Date: May 25, 2022.

This work was performed under the auspices of the U.S. Department of Energy by Lawrence Livermore National Laboratory under Contract DE-AC52-07NA27344 (LLNL-JRNL-812073).

model as well as the sensitivity to changes in this parameter. To reduce the uncertainty of the system, we may further improve the model by utilizing observational data in a Bayesian framework. That is, data related to the model output, as well as information about the model may be combined to learn the probability distribution of the variable coefficient.

For large-scale applications, common methods to perform Bayesian inference are infeasible. With the refinement of the spatial discretization scheme, both forming realizations of these random fields and performing forward PDE simulations are computationally demanding, as many approaches do not scale with the increase in problem size; furthermore, Bayesian inference approaches are typically limited to Markov chain Monte Carlo (MCMC) [48, 37, 52], and its variants, which require a large number of simulations as the parameter space is explored. However infeasible this approach may be, MCMC methods still lie at the root of many nonlinear Bayesian inference algorithms due to ease of implementation as well as the ability to apply in a blackbox fashion.

Over the recent decades new MCMC approaches have been developed to accelerate the parameter space exploration, in some cases allowing users to perform nonlinear Bayesian inference on large-scale applications. Notable approaches include those which utilize local approximations of the Hessian and gradient to modify the MCMC proposal [47, 51, 23, 24, 16, 10]. This method, dubbed, stochastic Newton MCMC, was shown in [51] to accelerate mixing; however, it requires gradient and Hessian information in addition to having solvers for the forward PDE and adjoint PDE models, as opposed to simply having the forward PDE model.

Another class of approaches include delayed acceptance MCMC algorithms, which utilize cheaper model approximations to accelerate the parameter search (also via proposal distribution modification) [18]. Several works have been completed that develop and explore the use of cheaper models with coarser spatial discretizations in a two-stage or multilevel framework. Early works that employ coarser spatial discretizations include [40] and [29]; the former utilizes a Metropolis coupled MCMC to swap proposals between coarse and fine chains, and the latter performs a delayed acceptance where sample proposals are only completed with the fine grid solver if their associated coarse grid solutions have been accepted. More recent works have investigated multilevel MCMC approaches. In particular, [27] developed an approach to both accelerate the mixing of the MCMC chain by using multiple levels, each with coarser spatial discretizations, and accelerate the sampling by performing variance reduction via multilevel Monte Carlo following the ideas of [38, 34, 8, 19, 56]. Analysis of a multilevel MCMC was completed in [41]. While promising speed up results have been shown, numerical testing has been limited to 2D spatial domains.

Aside from the computationally demanding forward models, a major set-back in these multilevel approaches, that has limited the size of the spatial domain to 2D, is the generation of the Gaussian random field realizations. In particular, all these works utilize a Karhunen-Loève (KL) expansion to model the unknown spatially correlated field that serves as a simulation input. For large-scale problems this can be computationally challenging, as doing so requires the calculation of the eigenvalues and eigenfunctions of the associated covariance function, which for standard approaches, will not scale with an increasingly refined spatial domain.

An alternative scalable approach to generate random field realizations is via a stochastic PDE – the reaction-diffusion equation – formulated in [57] and solved with finite elements in

[46], whereby each independent realization requires solving the stochastic PDE with an independent realization of spatial white noise function serving as the righthand side. Applying this approach in a multilevel setting, such as multilevel Monte Carlo or multilevel MCMC requires forming coupled random field realizations – and more specifically, spatial white noise – on multiple levels of discretization. A few works have completed this, including [28] which couples the fine and coarse level realizations to perform massively parallel multilevel Monte Carlo. In [49, 50] the authors solve a mixed PDE on the space of piecewise constants, and generate matching fine and coarse realizations by restricting the fine grid spatial white noise to the coarse level, using operators and solvers from element agglomerated algebraic multigrid (AMGe). In [21] the authors couple the coarse and fine level realizations using the primal formulation of the PDE.

While these approaches have been incorporated successfully into the multilevel Monte Carlo framework, they will not be useful for the multilevel MCMC framework. This is because in the aforementioned stochastic PDE approaches, the fine and coarse level realizations are coupled across the two levels. For example, in [49, 50], the fine level realizations are formed by sampling the spatial white noise source function on the fine level (to form the fine level Gaussian random field realization), and then the corresponding coarse realizations are formed by restricting the fine spatial white noise source function to the coarse level (to form the coarse level Gaussian random field realization). It is the opposite case in the multilevel MCMC approach – we must first sample from the coarse level, and then form a fine level random field in a hierarchical manner from the coarse realization. As this sampling approach has not yet been developed (to the best of the authors’ knowledge), this paper seeks to fill this void.

1.1. Contributions of this Work. In this work, we develop a scalable, hierarchical Gaussian random field sampling approach that complements the multilevel MCMC framework of [27] (though it may be applied to other two-level MCMC or delayed acceptance MCMC approaches discussed earlier). This approach works by forming a hierarchical decomposition of the white noise source function across multiple levels. To do this, we utilize the finite element solvers from [50] to solve the mixed formulation of the PDE-based approach of [57, 46]. In the approach of [50], each random field realization is formed by first sampling an independent realization of spatial white noise, then solving a mixed reaction-diffusion PDE where the white noise serves as a source function (the righthand side). In our work, we take a similar approach, but use L^2 projections to create a hierarchical decomposition of the white noise across discretization levels. An important clarification is that the work of [49, 50] has a different hierarchical approach; namely their sampling techniques generates realizations across the levels from a single fine level realization of white noise that is then restricted to the desired (coarser) level, e.g., using a nested hierarchy. In this work, our hierarchical approach allows us to form a direct decomposition of the white noise across all levels, whereby we may first sample on the coarsest level, and then add in white noise to the complementary spaces. By decomposing the white noise on the different discretizations in such a way, we are able to utilize this approach within a multilevel MCMC algorithm (see, e.g., [27]) for large-scale applications.

To present this new approach to hierarchical sampling, this paper is organized into the following sections. In Section 2, mathematical notation relevant to Gaussian random fields is presented to provide a framework for this sampling approach. In addition this section

TABLE 1. Mathematical Notation.

Variable	Description
$\mathbf{x} \in D \subset \mathbb{R}^d$	Point in spatial domain, $d = 2$ or 3
$\omega \in \Omega$	Outcome of Sample Space
$u \in \Theta := L^2(D)$	L^2 function defined over D
$\zeta := \zeta(\mathbf{x}, \omega)$	White noise function in D
$\mathbf{q} \in \mathbf{R} := H(\text{div}; D)$	$H(\text{div})$ function defined over D
Discrete Variable	
h, H	Subscripts to denote fine and coarse level objects
ℓ	Subscript denoting running level ℓ index, with $\ell = 0$ as finest
k	Subscript denoting target level of an algorithm
\mathcal{T}_ℓ	Level ℓ finite element triangulation
$u_\ell \in \Theta_\ell$	Piecewise constant function defined on \mathcal{T}_ℓ
\mathcal{Q}_ℓ	Orthogonal projection from L^2 to Θ_ℓ
P_ℓ	Interpolation operator mapping between $\Theta_{\ell+1}$ and Θ_ℓ
Π_ℓ	Restriction operator mapping between Θ_ℓ and $\Theta_{\ell+1}$
ζ_ℓ	White noise representation in Θ_ℓ
ζ_ℓ	Coefficient vector of white noise finite element representation in Θ_ℓ
ξ_ℓ	Vector of random elements
b_ℓ	Vector representation of white noise in Θ_ℓ
$\mathbf{q}_\ell \in \mathbf{R}_\ell$	Function of the lowest order Raviat-Thomas space on \mathcal{T}_ℓ
M_ℓ, B_ℓ, W_ℓ	Mass matrices for various level ℓ spaces

presents the stochastic PDE approach to calculating discrete Gaussian random field realizations. Our new hierarchical approach is presented in Section 3; this includes the theoretical aspects of performing a hierarchical direct decomposition of white noise – in a two-level and multilevel framework – resulting in a hierarchical approach to form Gaussian random field realizations. These aspects are presented in Lemma 3.2 and Theorem 3.1. The numerical implementation is discussed in Section 4, in the form of algorithms, as well as visualizations of the random field hierarchical decomposition. Numerical results are provided in Sections 5 and 6. Section 5 explores the cost and scaling of our multilevel hierarchical sampling technique applied to the Egg Model [43] using three levels; in particular, we show that the fine level scales with increased problem size. Section 6 incorporates this new hierarchical sampling technique into a three-level MCMC following the approach of [27], and shows that we obtain similar improvements in the multilevel acceptance rate, variance decay, and total computational cost when compared to the single-level approach.

1.2. Mathematical Notation. As a reference to the reader, we define the majority of this paper’s notation in Table 1. The first section of the table introduces general variables that provide a basis for the majority of the mathematical notation. The second section of the table refers to discrete variables that are used in various finite element representations, and that are frequently referred to throughout this work.

2. GAUSSIAN RANDOM FIELDS

In this work we consider a particular class of random fields, that is, spatially correlated Gaussian random fields, which in this context, will be used to describe an uncertain physical

process. Define the probability space $(\Omega, \mathcal{F}, \mathbb{P})$, with sample space Ω , σ -algebra \mathcal{F} , and probability \mathbb{P} . Given the spatial domain of interest $D \subset \mathbb{R}^d$, with $d = 2, 3$, we seek to form random field realizations of $\{u(\mathbf{x}, \omega) \in L^2(D) : \mathbf{x} \in D, \omega \in \Omega\}$, that follow a Gaussian prior density $u \sim \mathcal{N}(0, \mathcal{C})$ with zero mean and covariance operator \mathcal{C} . To ensure the mesh independent statistics of the random field u , \mathcal{C} is a trace-class operator [55]. Specifically, we define the covariance operator as the squared inverse elliptic operator (see e.g. [31, 15, 51]). That is,

$$(1) \quad \mathcal{C} = \mathcal{A}^{-2} \text{ with } \mathcal{A}u := -\operatorname{div} \left(\frac{1}{g} \nabla u \right) + \frac{\kappa^2}{g} u,$$

where κ denotes the inverse of the correlation length and g controls the marginal variance of the field. Using the above notation, we then define the probability density function as

$$(2) \quad d\mu(u) \propto \exp \left(-\frac{1}{2} \langle \mathcal{A}u, \mathcal{A}u \rangle \right),$$

where $\langle \mathcal{A}u, \mathcal{A}u \rangle = \int_D (\mathcal{A}u)^2 d\mathbf{x}$.

As described in [57, 46], for unbounded domains $D := \mathbb{R}^d$, the covariance operator (1) leads to Gaussian random field of the Matérn family with smoothness parameter ν and marginal variance σ^2 respectively given by

$$\nu = 2 - \frac{d}{2} \text{ and } \sigma^2 = \frac{g^2 \Gamma(\nu)}{\Gamma(\nu + d/2) (4\pi)^{d/2} \kappa^{2\nu}}.$$

In particular, in three-spatial dimensions, this gives the well-known exponential covariance operator

$$(\mathcal{C}u)(\mathbf{x}) := \int_D \operatorname{cov}(\mathbf{x}, \mathbf{y}) u(\mathbf{y}) d\mathbf{y}, \text{ with } \operatorname{cov}(\mathbf{x}, \mathbf{y}) := \frac{g^2}{8\pi\kappa} \exp(-\kappa \|\mathbf{x} - \mathbf{y}\|_2).$$

For a finite domains $D \subset \mathbb{R}^d$, suitable boundary conditions need be stipulated to reduce boundary artifacts, see e.g. [53, 44, 25]. In this work, we choose to extend the domain D to a larger domain $\bar{D} \subset \mathbb{R}^d$ and equip \mathcal{A} with homogeneous Neumann boundary conditions on $\partial\bar{D}$, as described in [50].

For sample-based UQ approaches—such as standard Monte Carlo—we desire to generate samples of this random field $u(\mathbf{x}, \omega)$ to serve as input field data to a model of interest. In our application (which we further detail in Section 6), we wish to generate permeability field realizations, $k = \exp[u(\mathbf{x}, \omega)]$, each which serves as an input to Darcy’s equations. While forming realizations of u can be done in a manner of ways, including via a KL expansion [33], circulant embedding [36], and a stochastic PDE approach [57, 46], all previous multilevel MCMC approaches has only considered sampling of random fields based on KL expansion [27, 30].

2.1. A KL Expansion for Sampling Random Fields. The KL expansion is a spectral decomposition that provides a natural way to introduce a hierarchy to random field realizations [33]. In particular, we may generate an approximate realization of $u(\mathbf{x}, \omega)$ by calculating the eigenvalues λ_i and eigenfunctions $\phi_i(\mathbf{x})$ of \mathcal{C} . Then for a fixed ω , and selected truncation value R , we define

$$(3) \quad u_{KL}(\mathbf{x}, \omega) = \sum_{i=1}^R \sqrt{\lambda_i} \phi_i(\mathbf{x}) \xi^{(i)}(\omega),$$

with each $\xi^{(i)}(\omega)$ independent and identically distributed (i.i.d.) $\mathcal{N}(0, 1)$. Above, the value of R controls the approximation error of $u_{KL}(\mathbf{x}, \omega)$; however, for rapidly decaying eigenvalues λ_i , R need not be exceedingly large to approximate a random field.

All work in multilevel MCMC with application to PDEs with random (spatially correlated) coefficients utilize the KL expansion to describe the random field [27, 30]. In particular, level-dependent truncation may be applied, as in [35, 56], to decompose the modes of (3) in such a way that the first set of modes may be associated with the random field on a coarse mesh, and then additional (complementary) modes associated with the random field on more refined meshes, so that the KL expansion may be defined in a hierarchical multilevel fashion.

A set-back, however, of the KL expansion approach, is the calculation of the eigenvalues and eigenfunctions of the covariance function. A straightforward, though perhaps naïve implementation, will have a cost that grows cubically with the degrees of freedom associated with the spatial discretization, i.e., the mesh size. While there are tools to improve this scaling, e.g., hierarchical matrix formations [9], storage and the ability to calculate the KL expansions for unstructured meshes are roadblocks to large-scale and extreme-scale applications. Due to the nature of our applications, that is, large-scale problems with unstructured meshes, we consider a stochastic PDE approach to generate Gaussian random field realizations.

2.2. A Stochastic PDE Approach for Finite Element Random Fields. As presented in [31, 15, 51], a realization of a Gaussian random field, with covariance operator \mathcal{C} given by (1), can be generated by solving the stochastic reaction-diffusion PDE

$$\mathcal{A}u = \zeta,$$

where $\zeta := \zeta(\mathbf{x}, \omega)$ is spatial Gaussian white noise. The spatial Gaussian white noise ζ is an $L^2(D)$ -bounded generalized function [46, Appendix B], such that

$$(4) \quad \langle \zeta, v \rangle \sim \mathcal{N}(0, \|v\|_{L^2(D)}^2) \quad \forall v \in L^2(D).$$

In the following, we consider a particular PDE-based approach that uses a mixed formulation to generate field realizations. That is, we follow the approach of [49, 50], which allows us to work in the space of piecewise constants. For large-scale applications this is beneficial as it provides a natural way to define spatial white noise, and the associated mass matrix is easily diagonalizable.

2.2.1. A Mixed Formulation. The following mixed stochastic PDE used in [49, 50] provides a way to generate Gaussian random field realizations: For a fixed $\omega \in \Omega$, a realization $u := u(\mathbf{x}, \omega)$ is calculated by solving the stochastic PDE:

$$(5) \quad \begin{aligned} (\boldsymbol{\rho}, \mathbf{s}) + (\operatorname{div} \mathbf{s}, u) &= 0 & \forall \mathbf{s} \in H(\operatorname{div}) \\ (\operatorname{div} \boldsymbol{\rho}, v) - \kappa^2 (u, v) &= -g \langle \zeta, v \rangle & \forall v \in L^2, \end{aligned}$$

where (\cdot, \cdot) denotes the $L^2(D)$ inner product. Above, the spatial Gaussian white noise $\zeta := \zeta(\mathbf{x}, \omega)$ is a zero-mean random Gaussian field on D such that $\langle \zeta, v \rangle \sim \mathcal{N}(0, \|v\|_{L^2(D)}^2)$, for any function $v \in L^2(D)$ (see (4)). Properties of finite element white noise will be discussed in the following section.

Define the spaces $\Theta = L^2(D)$ with inner product $(u, v) = \int_D uv d\mathbf{x}$ for all $u, v \in \Theta$ and $\mathbf{R} = H(\operatorname{div}; D) := \{\mathbf{q} \in [L^2(D)]^d \mid \operatorname{div} \mathbf{q} \in L^2(D), \mathbf{q} \cdot \mathbf{n} = 0 \text{ on } \partial D\}$ with inner product $(\mathbf{q}, \mathbf{s}) = \int_D \mathbf{q} \cdot \mathbf{s} d\mathbf{x}$ for all $\mathbf{q}, \mathbf{s} \in \mathbf{R}$. Let \mathbf{R}_h, Θ_h be the pair of the lowest order Raviart-Thomas spaces associated with the given triangulation \mathcal{T}_h .

For a fixed $\omega \in \Omega$, discrete solutions $\boldsymbol{\rho}_h \in \mathbf{R}_h$ and $u_h \in \Theta_h$ are calculated from the mixed system,

$$(6) \quad \begin{aligned} (\boldsymbol{\rho}_h, \mathbf{s}_h) + (\operatorname{div} \mathbf{s}_h, u_h) &= 0 & \forall \mathbf{s}_h \in \mathbf{R}_h \\ (\operatorname{div} \boldsymbol{\rho}_h, v_h) - \kappa^2 (u_h, v_h) &= -g \langle \zeta, v_h \rangle & \forall v_h \in \Theta_h. \end{aligned}$$

As we are in Θ_h , and the moments of ζ are well-defined for functions in Θ_h , we can define the mapping $\mathcal{Q}_h : \zeta \mapsto \mathcal{Q}_h \zeta \in \Theta_h$, where $\mathcal{Q}_h \zeta = \sum_{\tau \in \mathcal{T}_h} \zeta_\tau \chi_\tau$, and $\{\chi_\tau\}$ form the basis of Θ_h . That is, the random coefficients $\boldsymbol{\zeta}_h = (\zeta_\tau)_{\tau \in \mathcal{T}_h}$ are defined from the identity

$$(\mathcal{Q}_h \zeta, v_h) = \langle \zeta, v_h \rangle \quad \forall v_h \in \Theta_h.$$

The above identity is used to provide realizations of the white noise on a given finite element mesh \mathcal{T}_h . For this to be feasible, we need to study the properties of the random coefficients $\boldsymbol{\zeta}_h = (\zeta_\tau)$. The latter means that we can use the following expansion

$$\mathcal{Q}_h \zeta = \sum_{\tau \in \mathcal{T}_h} \zeta_\tau \chi_\tau,$$

where $\{\chi_\tau\}$ is an L^2 -orthogonal basis of piecewise constants spanning Θ_h , and the coefficients $\boldsymbol{\zeta}_h = (\zeta_\tau)$ are sampled from a particular distribution (to be specified later).

In what follows, for that particular distribution, we will refer to $\boldsymbol{\zeta}_h$, as a finite element representation of the white noise on \mathcal{T}_h .

2.2.2. Finite Element Representation of White Noise. To generalize, we first consider the situation of non-orthogonal basis $\{\phi_{h,i}\}_{i=1}^n$ of Θ_h , and change the notation accordingly. Consider the white noise representation with this non-orthogonal basis:

$$(7) \quad \zeta_h = \sum_{i=1}^n \zeta_i \phi_{h,i}.$$

The coefficient vector $\boldsymbol{\zeta}_h = (\zeta_i)$ is defined via the system with the mass matrix $W_h = ((\phi_{h,j}, \phi_{h,i}))_{i,j=1}^n$, i.e.,

$$W_h \boldsymbol{\zeta}_h = (\langle \zeta, \phi_{h,i} \rangle)_{i=1}^n.$$

To generate realizations of white noise in Θ_h , we consider the following properties (see [6, Section 1.4.3] and [7, Section 2.4.5] for details).

Property 2.1 (White noise in Θ_h). *Let ζ be white noise in D . Then, for the projection of ζ onto the basis $\{\phi_{h,i}\}_{i=1}^n$ of Θ_h , denoted ζ_h as in (7), it follows that,*

$$\mathbb{E}[(\zeta_h, \phi_{h,i})] = \mathbb{E}[\langle \zeta, \phi_{h,i} \rangle] = 0,$$

and

$$\mathbb{E}[(\zeta_h, \phi_{h,i})(\zeta_h, \phi_{h,j})] = \mathbb{E}[\langle \zeta, \phi_{h,i} \rangle \langle \zeta, \phi_{h,j} \rangle] = (\phi_{h,i}, \phi_{h,j}),$$

which implies

$$\mathbb{E}[(\zeta_h, \phi_{h,i})_{i=1}^n ((\zeta_h, \phi_{h,i})_{i=1}^n)^T] = ((\phi_{h,i}, \phi_{h,j}))_{i,j=1}^n = W_h,$$

for associated mass matrix W_h .

These properties follow from the theoretical aspects of white noise. Specifically, the covariance between two volumes A and B (within D) is equivalent to the mass of the intersection of the two volumes (further theoretical aspects of Gaussian white noise may be found in [6, 7]), and for finite element white noise this implies that the covariance is equivalent to the

mass matrix. Using the above properties, we can show that for $W_h \zeta_h$ to be a realization of Gaussian white noise, we require $\zeta_h = (\zeta_i)_{i=1}^n \sim \mathcal{N}(0, W_h^{-1})$.

Lemma 2.1. *Given the basis $\{\phi_{h,i}\}_{i=1}^n$ of Θ_h , associated mass matrix $W_h = ((\phi_{h,j}, \phi_{h,i}))_{i,j=1}^n$, and $\zeta_h = (\zeta_i)_{i=1}^n$ sampled from $\mathcal{N}(0, W_h^{-1})$, it follows that $W_h \zeta_h$ is a realization of white noise in Θ_h .*

Proof. Following Property 2.1, it is sufficient to show that $\mathbb{E}[W_h \zeta_h] = 0$ and $\mathbb{E}[W_h \zeta_h (W_h \zeta_h)^T] = W_h$. As $\zeta_h \sim \mathcal{N}(0, W_h^{-1})$, it is clear that $\mathbb{E}[W_h \zeta_h] = 0$. As for the covariance, we have

$$\begin{aligned} \mathbb{E}[W_h \zeta_h (W_h \zeta_h)^T] &= W_h \mathbb{E}[\zeta_h \zeta_h^T] W_h \\ &= W_h W_h^{-1} W_h \\ &= W_h. \end{aligned}$$

□

Now we return to the specific case used in this work, where we have the L^2 -orthogonal basis of piecewise constants, $\{\chi_\tau\}$, spanning Θ_h . The righthand side of (6), which is the moment $\langle \zeta, v_h \rangle$, is now evaluated for each basis function $v_h = \chi_\tau$. Using the equivalence $\langle \zeta, v_h \rangle = (\mathcal{Q}_h \zeta, v_h)$ for $v_h \in \Theta_h$, and the expansion $\zeta_h = \mathcal{Q}_h \zeta = \sum_{\tau \in \mathcal{T}_h} \zeta_\tau \chi_\tau$, it follows that the righthand side will have the coefficient vector $b_h \equiv ((\zeta_h, \chi_\tau))_{\tau \in \mathcal{T}_h}$. As a consequence of using piecewise constant basis functions, each inner product simplifies as

$$(\zeta_h, \chi_\tau) = \zeta_\tau \|\chi_\tau\|^2.$$

In other words, $b_h = W_h \zeta_h$, with W_h now a diagonal mass matrix.

2.2.3. Finite Element Representation of Gaussian Random Fields. In the actual computation of u_h , we use the equivalent vector representation for the righthand side of (6), defined as

$$(8) \quad -gb_h = -gW_h^{\frac{1}{2}} \xi_h,$$

with $\xi_h \sim \mathcal{N}(0, I)$. We note this equivalence is made clearer in Section 4. As we are in the space of piecewise constants in L^2 , the square root of the mass matrix W_h is easily calculated. Let M_h be the mass matrix associated with inner product (ρ_h, \mathbf{s}_h) and B_h the mass matrix associated with the bilinear form $(\text{div } \mathbf{s}_h, u_h)$. Then the matrix representation of (6) is given as

$$(9) \quad \begin{bmatrix} M_h & B_h^T \\ B_h & -\kappa^2 W_h \end{bmatrix} \begin{bmatrix} \rho_h \\ u_h \end{bmatrix} = \begin{bmatrix} \mathbf{0} \\ -gb_h \end{bmatrix},$$

with b_h defined by (8).

For ease of notation, we introduce the scaled negative Schur Complement of (9) defined by

$$(10) \quad A_h := \frac{\kappa^2}{g} W_h + \frac{1}{g} B_h M_h^{-1} B_h^T.$$

As demonstrated in [49], solutions u_h of the mixed system in (9) are discrete realizations of a Gaussian random field with density $\mu_h \sim \mathcal{N}(\mathbf{0}, C_h)$, where $C_h = A_h^{-1} W_h A_h^{-1}$. It then follows that the corresponding probability density function is

$$(11) \quad \mu_h(u_h) \propto \exp(-u_h^T A_h W_h^{-1} A_h u_h) = \exp(-b_h^T W_h^{-1} b_h).$$

3. MULTILEVEL HIERARCHICAL DECOMPOSITION OF FINITE ELEMENT WHITE NOISE

In what follows we study the computational aspects of sampling the righthand side in (6) from a coarse finite element space $\Theta_H \subset \Theta_h$, and its (direct) hierarchical complement space $(I - \mathcal{Q}_H)\Theta_h$, where $\mathcal{Q}_H : L^2 \mapsto \Theta_H$ is the corresponding L^2 -projection. For any $\zeta_h \in \Theta_h$, we use the two-level hierarchical decomposition

$$\zeta_h = \mathcal{Q}_H \zeta_h + (I - \mathcal{Q}_H) \zeta_h$$

to decompose ζ_h into the spaces Θ_H and $\Theta_h \setminus \Theta_H$. Since we work with spaces of discontinuous (piecewise constant) functions Θ_h and Θ_H with associated mass matrices W_h and W_H , respectively, the projection \mathcal{Q}_H is easily implemented (by inverting a diagonal (coarse) mass matrix).

Define P to be the interpolation matrix that relates the coarse coefficient vector ζ_H of ζ_H (expanded in terms of the basis of Θ_H) and the fine coefficient vector ζ_h of $\zeta_h \in \Theta_H \subset \Theta_h$ expanded in terms of the basis of Θ_h . That is,

$$\zeta_h = P \zeta_H.$$

Let $\Pi = W_H^{-1} P^T W_h$ denote the restriction operator, then $P \Pi$ is the matrix representation of \mathcal{Q}_H and $\Pi P = I$. That is, we have $P \zeta_H = P \Pi \zeta_h$, or $\zeta_H = \Pi \zeta_h$.

In what follows, we first seek to show that $\mathcal{Q}_H \zeta_h$ gives rise to a coarse random coefficient vector $\zeta_H \sim \mathcal{N}(0, W_H^{-1})$.

Lemma 3.1. *Let $\zeta_h \in \Theta_h$, with coefficient vector $\zeta_h \sim \mathcal{N}(0, W_h^{-1})$. Then $\zeta_H \equiv \mathcal{Q}_H \zeta_h$ has coefficient vector $\zeta_H \sim \mathcal{N}(0, W_H^{-1})$.*

Proof. Given the associated coarse coefficient $\zeta_H = \Pi \zeta_h$ with $\zeta_h \sim \mathcal{N}(0, W_h^{-1})$, it is clear the mean is zero. For the covariance matrix, we have

$$\begin{aligned} \mathbb{E}[\zeta_H \zeta_H^T] &= \mathbb{E}[\Pi \zeta_h (\Pi \zeta_h)^T] \\ &= W_H^{-1} P^T W_h \mathbb{E}[\zeta_h \zeta_h^T] W_h P W_H^{-1} \\ &= W_H^{-1}. \end{aligned}$$

Above, we use $\mathbb{E}[\zeta_h \zeta_h^T] = W_h^{-1}$ and the Galerkin relation between the coarse and the fine level mass matrices, $W_H = P^T W_h P$. \square

Therefore, if ζ_h has coefficient vector $\zeta_h \sim \mathcal{N}(0, W_h^{-1})$ then the same holds for the coarse projection $\zeta_H = \mathcal{Q}_H \zeta_h$, that is, its coefficient vector $\zeta_H = \Pi \zeta_h \sim \mathcal{N}(0, W_H^{-1})$. In other words, if ζ_h is a fine finite element representation of white noise, then its projection $\zeta_H = \mathcal{Q}_H \zeta_h$ is the corresponding coarse finite element representation of white noise.

Next we present our main lemma, which allows us to utilize this two-level, hierarchical decomposition to form a realization of white noise on Θ_h . We highlight that this construction is crucial for multilevel MCMC, as we consider the coarse and fine representations of white noise to be formed independently, where their resulting combination (in this hierarchical manner) is a fine representation of white noise.

Lemma 3.2. *Let $\zeta_H \in \Theta_H$ be a coarse representation of white noise with a coarse coefficient vector $\zeta_H \sim \mathcal{N}(0, W_H^{-1})$, and let $\zeta_h \in \Theta_h$ be a fine representation of white noise with fine coefficient vector $\zeta_h \sim \mathcal{N}(0, W_h^{-1})$, such that ζ_H and ζ_h are independent. Then the fine level function*

$$(12) \quad \zeta'_h = \zeta_H + (I - \mathcal{Q}_H) \zeta_h$$

is a representation of the white noise in Θ_h .

Proof. First, consider the coefficient vector of ζ'_h , given as

$$(13) \quad \zeta'_h = P\zeta_H + (I - P\Pi)\zeta_h.$$

To prove ζ'_h is a representation of Gaussian white noise, we must show Definition 2.1 holds, that is $\mathbb{E}[\zeta'_h] = 0$, and $\mathbb{E}[\zeta'_h(\zeta'_h)^T] = W_h^{-1}$. We assume that ζ_H and ζ_h are independent, which implies that $\mathbb{E}[\zeta_H\zeta_h^T] = \mathbb{E}[\zeta_H]\mathbb{E}[\zeta_h^T] = 0$. Hence for the covariance matrix, we have

$$\begin{aligned} \mathbb{E}[\zeta'_h(\zeta'_h)^T] &= \mathbb{E}[(P\zeta_H + (I - PW_H^{-1}P^TW_h)\zeta_h)(P\zeta_H + (I - PW_H^{-1}P^TW_h)\zeta_h)^T] \\ &= P\mathbb{E}[\zeta_H\zeta_H^T]P^T + (I - PW_H^{-1}P^TW_h)\mathbb{E}[\zeta_h\zeta_h^T](I - W_hPW_H^{-1}P^T) \\ &= PW_H^{-1}P^T + (I - PW_H^{-1}P^TW_h)W_h^{-1}(I - W_hPW_H^{-1}P^T) \\ &= W_h^{-1}. \end{aligned}$$

That is, $\zeta'_h \sim \mathcal{N}(0, W_h^{-1})$; hence ζ'_h is a fine finite element representation of white noise. It is clear also that $\zeta_H = \mathcal{Q}_H\zeta'_h$ and $(I - \mathcal{Q}_H)\zeta_h = (I - \mathcal{Q}_H)\zeta'_h$. \square

In conclusion, the finite element hierarchical (direct) decomposition based on \mathcal{Q}_H provides a hierarchical decomposition of the fine finite element white noise into a coarse finite element representation of white noise plus a computational hierarchical (direct) complement which also involves fine finite element representation of white noise.

3.1. The multilevel hierarchical decomposition. Next we wish to extend the above two-level hierarchical decomposition of Gaussian white noise to a multilevel hierarchical decomposition, so that we may sample across multiple levels of discretization.

Let $\mathcal{T}_0 \equiv \mathcal{T}_h$ denote the finest level triangulation of D , with a hierarchy of L coarser levels given as $\{\mathcal{T}_\ell\}_{\ell=1}^L$, such that \mathcal{T}_L represents the coarsest triangulation. We consider the finite element space Θ_ℓ to be the space of piecewise constant functions associated with the triangulation \mathcal{T}_ℓ , for $\ell = 0, \dots, L$, and with mass matrix W_ℓ ; and \mathbf{R}_ℓ the lowest order Raviart-Thomas space associated with the triangulation \mathcal{T}_ℓ . Additionally, define the sequence of L^2 -projections $\mathcal{Q}_\ell : L^2 \mapsto \Theta_\ell$ with $\ell = 0, \dots, L$.

In what follows, we construct the multilevel hierarchical decomposition of white noise for a given level $k < L$.

Theorem 3.1. *Consider the representations of white noise, given as $\zeta_\ell \in \Theta_\ell$ with associated coefficient vectors $\zeta_\ell \sim \mathcal{N}(0, W_\ell^{-1})$, for $\ell = k, \dots, L$, such that each ζ_ℓ is independent. Then the level k function*

$$(14) \quad \zeta'_k = \zeta_L + \sum_{\ell=k}^{L-1} (I - \mathcal{Q}_{\ell+1})\zeta_\ell,$$

with $k < L$, is a representation of the white noise in Θ_k .

Proof. First, consider the two-level decomposition. Let $\zeta_L \in \Theta_L$ be a realization of white noise from the coarsest level (level L). Given an independent realization of white noise from level $L - 1$, denoted $\zeta_{L-1} \in \Theta_{L-1}$, it follows from Lemma 3.2 that

$$\zeta'_{L-1} = \zeta_L + (I - \mathcal{Q}_L)\zeta_{L-1},$$

is a realization of white noise in Θ_{L-1} . To generate a realization on level $L - 2$, we simply sample independent white noise $\zeta'_{L-2} \in \Theta_{L-2}$, and form the hierarchical realization that

builds from our previous white noise realization ζ'_{L-1} :

$$\zeta''_{L-2} = \zeta'_{L-1} + (I - \mathcal{Q}_{L-1})\zeta'_{L-2},$$

which, by Lemma 3.1, is a realization of white noise in Θ_{L-2} . Continuing in this fashion to level k , let $\zeta_k^* \in \Theta_k$ be a sample of white noise that has been hierarchically formed. Let $\zeta_{k-1}^* \in \Theta_{k-1}$ be an independently sampled realization of level $k-1$ white noise. Then it follows from Lemma 3.1 that

$$\zeta_{k-1}^{**} = \zeta_{k-2}^* + (I - \mathcal{Q}_{k-2})\zeta_{k-1}^*,$$

is a realization of white noise in Θ_{k-1} . By induction, it follows that, for an arbitrary level ℓ , this hierarchical multilevel construction formulates a realization of white noise in Θ_ℓ . \square

The associated coefficient representation is defined similarly to (13); however, we replace the subscript h with k to denote the level, and let P_k be the interpolation matrix that maps the level $k+1$ coefficient vector ζ_{k+1} of ζ_{k+1} to the level k coefficient vector ζ_k of ζ_k , such that $\zeta_k = P_k \zeta_{k+1}$. This hierarchical coefficient representation (in two-level form) is given as

$$(15) \quad \zeta'_k = P_k \zeta_{k+1} + (I - P_k W_{k+1}^{-1} P_k^T W_k) \zeta_k.$$

Just as in the proof, we can hierarchically build a level k coefficient vector by starting on the coarsest level and adding on coefficients projected onto the complimentary spaces, as will be further detailed in the next section (see, e.g., Algorithm 4.1).

The multilevel, hierarchical decomposition in (14) provides the theoretical framework that allows us to decompose the white noise across multiple levels, enabling us to perform hierarchical sampling of Gaussian random field.

4. IMPLEMENTATION OF THE HIERARCHICAL SAMPLER

Here we present the finite element approach by which the hierarchical decomposition of white noise is formed, and the corresponding Gaussian random field realization u_k is calculated. Recall from Lemma 2.1 that we may sample (single-level) finite element white noise on level k via $W_k \zeta_k$ with $\zeta_k = (\zeta_i)_{i=1}^n \sim \mathcal{N}(0, W_k^{-1})$.

While we can use the decomposition in (15) for our hierarchical implementation, we instead rearrange this representation to accomplish two additional goals: first, that on each level we sample from a $\mathcal{N}(0, I)$ distribution, and second, that we utilize the interpolation and restriction operators P_k and Π_k .

To obtain a realization of white noise in the righthand side of (6), we require the product with W_k to obtain $W_k \zeta_k$. Applying this to the hierarchical representation of (15) results in:

$$W_k \zeta_k = W_k P_k \zeta_{k+1} + W_k (I - P_k W_{k+1}^{-1} P_k^T W_k) \zeta_k.$$

For algorithmic efficiency (and to meet our additional two goals), we simplify the above using the fact that $\zeta_k = W_k^{-1} W_k^{\frac{1}{2}} \xi_k$ with $\xi_k \sim \mathcal{N}(0, I)$ and $P_k^T (W_k^{\frac{1}{2}} \xi_k) = W_{k+1}^{\frac{1}{2}} \xi_{k+1}$ to get the new representation of hierarchical finite element white noise:

$$W_k^{\frac{1}{2}} \xi_k = \Pi_k^T (W_{k+1}^{\frac{1}{2}} \xi_{k+1}) + (I - \Pi_k^T P_k^T) (W_k^{\frac{1}{2}} \xi_k).$$

And now we have the decomposition of the righthand side of the discrete problem (6):

$$b_k = \Pi_k^T b_{k+1} + (I - \Pi_k^T P_k^T) b_k,$$

where, similarly to that in (8), we define $b_k = W_k^{\frac{1}{2}} \xi_k$.

In practice, we use the finite element white noise formulation of b_k , but construct a realization using all coarser levels, not only the $k + 1$ level. This process is described in Algorithm 4.1. For a given level k , we first calculate finite element white noise on the coarsest level L , denoted b_L . Then we iterate through each finer level, where we calculate b_ℓ by first interpolating the coarser $b_{\ell+1}$ (which was previously calculated), and then adding a spatial white noise realization that is complementary to the coarser $\ell + 1$ space – this is accomplished by multiplying level ℓ spatial white noise, $W_\ell^{1/2}\boldsymbol{\xi}_\ell$, with $(I - \Pi_\ell^T P_\ell^T)$, which projects the level ℓ spatial white noise orthogonal to the coarser space(s). After each iterate, we refine a level (decrease ℓ by 1), and repeat this process. This done until we reach level k , and the resulting b_k provides us with our hierarchically generated realization of spatial white noise, which can then be used in the righthand side of the discrete problem (6).

Algorithm 4.1: Form finite element white noise via new hierarchical approach.

<p>Input: Current level k (with $0 \leq k \leq L$), L, independent $\{\boldsymbol{\xi}_L, \boldsymbol{\xi}_{L-1}, \dots, \boldsymbol{\xi}_k\}$ with each $\mathcal{N}(\mathbf{0}, I_k)$</p> <p>$\ell = L$</p> <p>$b_L = W_L^{1/2}\boldsymbol{\xi}_L$</p> <p>$\ell = \ell - 1$</p> <p>while $\ell \geq k$ do</p> <table border="0"> <tr> <td style="padding-right: 10px;"> </td> <td>$b_\ell = \Pi_\ell^T b_{\ell+1} + (I - \Pi_\ell^T P_\ell^T)W_\ell^{1/2}\boldsymbol{\xi}_\ell$</td> </tr> <tr> <td style="padding-right: 10px;"> </td> <td>$\ell = \ell - 1$</td> </tr> </table> <p>end</p> <p>Output: $\{b_L, b_{L-1}, \dots, b_k\}$</p>		$b_\ell = \Pi_\ell^T b_{\ell+1} + (I - \Pi_\ell^T P_\ell^T)W_\ell^{1/2}\boldsymbol{\xi}_\ell$		$\ell = \ell - 1$
	$b_\ell = \Pi_\ell^T b_{\ell+1} + (I - \Pi_\ell^T P_\ell^T)W_\ell^{1/2}\boldsymbol{\xi}_\ell$			
	$\ell = \ell - 1$			

In this work we employ the same linear system of [49, Section 2.2], but instead of spatial white noise generated strictly on the fine level, we use our hierarchical approach. For a given level k , we seek to calculate solutions $(\boldsymbol{\rho}_k, u_k) \in \mathbf{R}_k \times \Theta_k$ via the linear system

$$(16) \quad \begin{bmatrix} M_k & B_k^T \\ B_k & -\kappa^2 W_k \end{bmatrix} \begin{bmatrix} \boldsymbol{\rho}_k \\ u_k \end{bmatrix} = \begin{bmatrix} 0 \\ -g b_k \end{bmatrix},$$

where M_k be the mass matrix associated with inner product $(\boldsymbol{\rho}_k, \mathbf{s}_k)$, W_k with the inner product (u_k, v_k) which is diagonal, B_k with the bilinear form $(\text{div } \mathbf{s}_k, u_k)$, and b_k is hierarchically generated spatial white noise (generated via Algorithm 4.1). For a scalable, parallelizable implementation, we have several solvers we may consider, one of which – hybridization AMG approach from [45, 26] – is amenable to large-scale applications because the the mass matrices need only be computed one time (on each level), and then may be reapplied to different realizations of b_k .

To define the Gaussian densities μ_k at level k we proceed as is Section 2.2.3. Let us formally introduce the negative scaled Schur Complement of (16) A_k defined as

$$A_k := \frac{\kappa^2}{g} W_k + \frac{1}{g} B_k M_k^{-1} B_k^T.$$

Then solutions of (16) are Gaussian random vectors with distribution $\mu_k \sim \mathcal{N}(0, A_k^{-1} W_k A_k^{-1})$ and corresponding probability density

$$\mu_k(u_k) \propto \exp(-u_k^T A_k W_k^{-1} A_k u_k) = \exp(-b_k^T W_k^{-1} b_k).$$

We also define the conditionally Gaussian density $u_k|u_{k+1}$ based on our hierarchical decomposition of white noise in Algorithm 4.1. Sampling from the prior distribution μ_k and from the conditional distribution $u_k|u_{k+1}$ are summarized in Algorithm 4.2 and Algorithm 4.3. These algorithms will be used to define the proposal distributions within the multilevel MCMC algorithm in Section 6.

Algorithm 4.2: Generate a sample u_k from the prior distribution μ_k at level k .

Input: Current level k (with $0 \leq k \leq L$)

Sample $\boldsymbol{\xi}_k \sim \mathcal{N}(\mathbf{0}, I_k)$

Define $b_k = W_k^{1/2} \boldsymbol{\xi}_k$

Compute u_k by solving (16)

Output: u_k

Algorithm 4.3: Generate a sample u_k from the conditional distribution $u_k|u_{k+1}$

Input: Current level k (with $0 \leq k < L$), the coarse level sample $u_{k+1} = A_{k+1}^{-1} b_{k+1}$

Sample $\boldsymbol{\xi}_k \sim \mathcal{N}(\mathbf{0}, I_k)$

Define $b_k = \Pi_k^T b_{k+1} + (I - \Pi_k^T P_k^T) W_k^{1/2} \boldsymbol{\xi}_k$

Compute u_k by solving (16)

Output: u_k

4.1. Random Field Realizations Using Hierarchical Components. To visualize the hierarchical components of a fine level solution u_0 , we consider the Egg model domain [43] using three levels of refinement with 18.5K, 148K, and 1.18M elements for levels $\ell = 2, 1$, and 0, respectively. Here we skip over the model details, as these will be addressed in the following section, and focus on the new hierarchical sampler.

Using Algorithm 4.1 with $k = 0$ and $L = 2$, we generate the three components of the righthand side given as $b_0 = \Pi_0^T \Pi_1^T W_2^{1/2} \boldsymbol{\xi}_2 + \Pi_0^T (I - \Pi_1^T P_1^T) W_1^{1/2} \boldsymbol{\xi}_1 + (I - \Pi_0^T P_0^T) W_0^{1/2} \boldsymbol{\xi}_0$. For visualization purposes, we separate these three components of b_0 and solve with each independently. That is, we seek solutions $u_0^{C\ell}$ via

$$(17) \quad \begin{aligned} A_0 u_0^{C2} &= \Pi_0^T \Pi_1^T W_2^{1/2} \boldsymbol{\xi}_2, \\ A_0 u_0^{C1} &= \Pi_0^T (I - \Pi_1^T P_1^T) W_1^{1/2} \boldsymbol{\xi}_1, \\ A_0 u_0^{C0} &= (I - \Pi_0^T P_0^T) W_0^{1/2} \boldsymbol{\xi}_0. \end{aligned}$$

Note that the fine level realization is simply $u_0 := u_0^{C2} + u_0^{C1} + u_0^{C0}$. Figure 1 (a)-(c) displays the solutions u_0^{C2} , u_0^{C1} , and u_0^{C0} . These results showcase the novelty of this hierarchical approach – that is, the finite element white noise decomposition enables a realization u_0 to be decomposed into independent components across multiple levels. Moreover, this hierarchical approach induces a separation of scales among the terms $u_0^{C\ell}$, similar to that induced by the hierarchical KL-based sampling in [27]. On the coarse levels, the terms $u_0^{C\ell}$ capture the smooth components of u_0 , while, on finer levels, the terms $u_0^{C\ell}$ only contain the highly oscillatory components of u_0 . This property plays a fundamental role in accelerating the mixing and reducing the variance of the multilevel MCMC in Section 6. This is clearly illustrated by considering the sums of the components $u_0^{C\ell}$ shown in Figure 1 (d)-(e). In

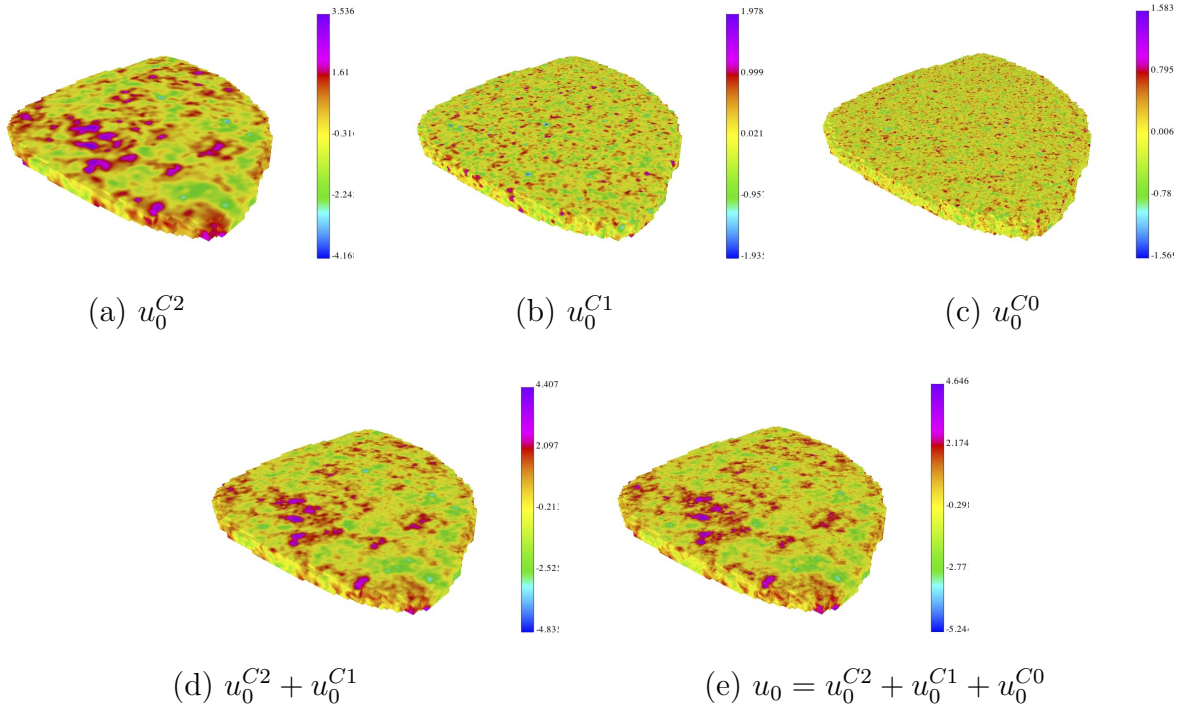


FIGURE 1. Various components of a realization u_0 on three levels as defined in (17), and generated from Algorithm 4.2 and Algorithm 4.3.

particular, Figure 1 (d) displays $u_0^{C2} + u_0^{C1}$, and Figure 1 (e) displays the complete fine level realization u_0 .

5. NUMERICAL RESULTS: MULTILEVEL HIERARCHICAL SAMPLE GENERATION

In this section, we test the hierarchical sampler scaling on the ‘Egg model’ [43], as it contains a large, irregular domain. The Egg domain is contained by a $480 \text{ m} \times 480 \text{ m} \times 28 \text{ m}$ bounding box. We note that, as we are employing the approach of [50], we require performing mesh embedding, that is, the Egg model domain is embedded within a $512 \text{ m} \times 512 \text{ m} \times 44 \text{ m}$ domain. This mitigates variance inflation along the boundary due to Neumann boundary conditions (see [46, Section 2.3] and [49, 50] for additional discussion). Figure 2 displays both the original Egg model mesh and enlarged mesh (in which it is embedded) for the coarsest level, both with hexahedral elements of size $8 \text{ m} \times 8 \text{ m} \times 4 \text{ m}$. Finer mesh resolutions are formed by uniformly refining by a factor of two in each direction.

To test the scaling, we consider three levels $\ell = 0, 1, 2$, with degrees of freedom (corresponding to the number of unknowns in the mixed PDE system as in (16)) given in Table 2 with $\text{NP} = 36$ total MPI processes; then, for a fixed problem size per processor, we increase the number of processes to $\text{NP} = 288$ and then $\text{NP} = 2304$. Gaussian random field realizations were generated following our new hierarchical PDE sampling approach; that is, for levels $\ell = 0, 1, 2$, level ℓ hierarchical white noise was sampled according to Algorithm 4.1, and realizations of u_ℓ were formed by solving the linear system in (16) on the Egg domain. Obtaining good scalability results requires access to well developed scalable solvers. Numerical simulations were performed using tools developed in ParELAG [4], a parallel C++ library

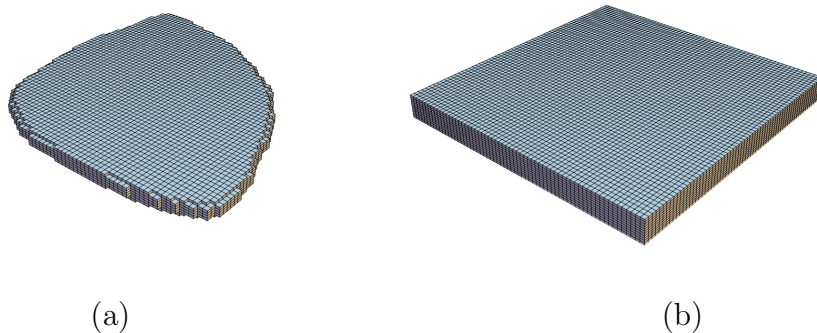


FIGURE 2. (a) Original Egg model mesh containing 18.5K elements. (b) Enlarged mesh, in which the Egg model mesh is embedded, extends two elements in each direction beyond the Egg model mesh bounding box, and contains 45K elements. Both meshes displayed correspond to the coarsest level.

TABLE 2. Number of global degrees of freedom (DOFs) associated with each level, for each set of process numbers. The DOFs here are associated with the number of unknowns in the mixed PDE system as in (16).

NP	DOFs $\ell = 0$	DOFs $\ell = 1$	DOFs $\ell = 2$
36	4.8063e+06	6.0788e+05	7.7758e+04
288	3.8223e+07	4.8063e+06	6.079e+05
2304	3.0488e+08	3.8223e+07	4.8063e+06

for performing numerical upscaling of finite element discretizations and AMG techniques, and ParELAGMC [5], a parallel element agglomeration MLMC library. These libraries use MFEM [3] to generate the fine grid finite element discretization and HYPRE [2] to handle massively parallel linear algebra. Visualizations are rendered with GLVis [1]. Note, all timing results were executed on the Quartz cluster at Lawrence Livermore National Laboratory, consisting of 2,688 nodes where each node has two 18-core Intel Xeon E5-2695 processors. For the weak scaling results, we use 36 MPI processes per node.

Figure 3 provides the weak scaling of this approach for generating 100 samples (see Figure 3 (a)), as well as the associated efficiency (see Figure 3 (b)) for each level and three sets of MPI processes NP as listed in Table 2. In Figure 3 (a) the computational time for the finest level, $\ell = 0$, remains relatively flat with the increase in NP, while the coarsest level, $\ell = 2$, has the worst scaling for the given number of processes. That said, it is still clear that the coarse level samples are faster to generate than the finest level samples. For the three levels, the associated efficiency of this scaling is provided in Figure 3 (b); with the finest level efficiency decreasing to 85% and 80% with the increase in NP, and the coarsest level decreasing to 50% and 25%. This is to be expected – with the increase in the number of processes, the coarser levels require greater communication time, which decreases the cost efficiency; however, it does indicate a drawback with our HPC implementation, that is, for

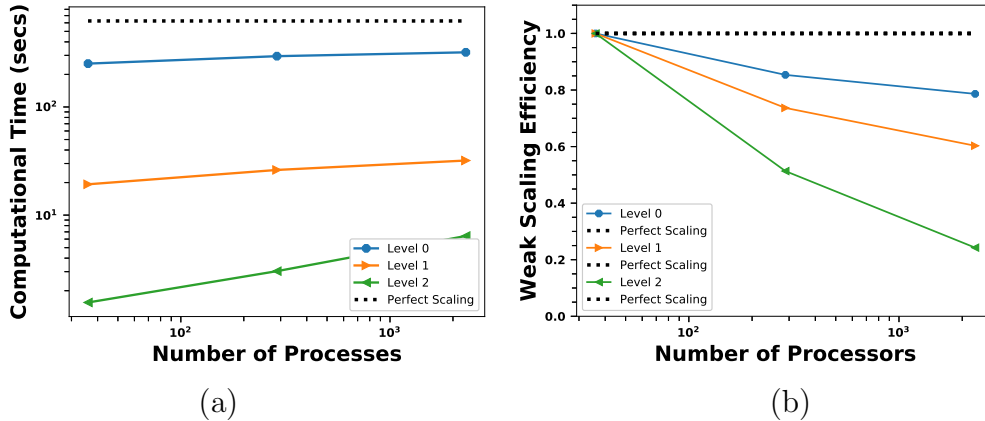


FIGURE 3. (a) Weak scaling for the three different levels; here levels refers to a fixed number of elements per processor. (b) Associated efficiency across the three levels.

coarser discretizations, we require fewer processes than the fine discretizations. Because of this, we are unable to get complete scaling across all levels; rather each level will benefit from a different number of processes. The work in [28] describes this as the *scalability window* – that is, each level has a range of NP values it can run on in order to maintain weak scaling efficiencies greater than a specified threshold – and investigates applying this approach to multilevel Monte Carlo. While this approach would greatly improve the scaling of this method, it is outside the scope of this paper.

6. HIERARCHICAL PDE APPROACH FOR MULTILEVEL MCMC

In this section, we apply the proposed hierarchical PDE-based sampling approach to solve a nonlinear Bayesian inference problem. We use the multilevel MCMC framework in [27] to explore the posterior distribution of the uncertain parameter and estimate moments (the mean) of a scalar quantity of interest Q .

In particular, we consider the problem of inferring a log-normal permeability field from cell-averaged pressure measurements for a single phase steady state subsurface problem. In what follows, we denote with $u \in \Theta$ the uncertain parameter representing the logarithm of the permeability field, with $(\mathbf{q}, p) \in \mathbf{R} \times \Theta$ the state variables representing the flow velocity and pressure, and with $p_{\text{obs}} \in \mathbb{R}^m$ the data representing cell-averaged pressure observations at m given measurement locations.

Prior distribution. We assume a Gaussian prior density on the spatially varying log-permeability coefficient, i.e. $u \sim \mathcal{N}(u_*, \mathcal{C})$, with covariance operator \mathcal{C} and mean value $u_* = 0$. To ensure that the inference problem is well-posed in infinite dimensions, we use a squared inverse elliptic operator in (1) to define the prior covariance operator, see for example [55, 31, 15, 51]. Samples from the prior distribution can then be drawn by solving (5) as we explained in Section 2.2, and their probability can be computed using (2).

Forward map. Let $y = \mathcal{F}(u)$ denote the forward map from the uncertain field $u \in \Theta$ to the observable $y \in \mathbb{R}^m$. The map $\mathcal{F} = \mathcal{B} \circ \mathcal{H}$ is the composition of a forward PDE solve \mathcal{H} that computes the pressure field p for a given realization of log-permeability u and a linear operator \mathcal{B} that evaluates the pressure p on local cells. For a single phase porous media flow, with $k = \exp(u)$, we define $p = \mathcal{H}(u)$ as the solution to the mixed formulation of the Darcy’s

equations

$$(18) \quad \begin{aligned} (k^{-1}\mathbf{q}, \mathbf{s}) - (\operatorname{div} \mathbf{s}, p) &= (\mathbf{f}, \mathbf{s}) \quad \forall \mathbf{s} \in \mathbf{R} \\ (\operatorname{div} \mathbf{q}, v) &= 0 \quad \forall v \in \Theta, \end{aligned}$$

with Dirichlet boundary condition $p = p_D$ on Γ_D , enforced by the right-hand side \mathbf{f} , and Neumann boundary condition $\mathbf{q} \cdot \mathbf{n} = 0$ on Γ_N , where Γ_D and Γ_N are non-overlapping partitions of ∂D .

Likelihood function. We assume that the measured data $p_{\text{obs}} \in \mathbb{R}^m$ are corrupted by additive Gaussian noise η with zero mean and covariance $\Gamma_\eta = \sigma_\eta^2 I_m$, where I_m is the identity matrix in \mathbb{R}^m . That is,

$$(19) \quad p_{\text{obs}} = \mathcal{F}(u) + \eta, \quad \eta \sim \mathcal{N}(0, \Gamma_\eta).$$

From the noise model in (19), we have that the conditional probability of p_{obs} given u is also Gaussian with mean $\mathcal{F}(u)$ and covariance Γ_η , that is

$$p_{\text{obs}}|u \sim \mathcal{N}(\mathcal{F}(u), \Gamma_\eta).$$

The likelihood function $\pi^{\text{like}}(p_{\text{obs}}|u)$ then reads

$$(20) \quad \pi^{\text{like}}(p_{\text{obs}}|u) \propto \exp\left(-\frac{1}{2}\|p_{\text{obs}} - \mathcal{F}(u)\|_{\Gamma_\eta^{-1}}^2\right),$$

where $\|\cdot\|_{\Gamma_\eta^{-1}}^2$ denotes the Γ_η^{-1} -weighted l^2 norm in \mathbb{R}^m .

Posterior distribution. By applying Bayes' theorem, the posterior density ν in the infinite dimensional case is given by

$$(21) \quad \nu(u|p_{\text{obs}}) \propto \pi^{\text{like}}(p_{\text{obs}}|u)d\mu(u),$$

where $\pi^{\text{like}}(p_{\text{obs}}|u)$ is the likelihood function in (20) and $d\mu(u)$ is the prior density in (2). We note that, although the prior distribution and likelihood functions are both Gaussian, the posterior distribution $\nu(u|p_{\text{obs}})$ is not Gaussian because of the nonlinearity introduced by the forward map \mathcal{F} . Thus, there is no closed form solution to the Bayesian inference problem and therefore we will use MCMC sampling to explore the posterior distribution.

Quantity of interest. Finally, let us introduce the scalar quantity of interest $Q = Q(u)$ representing the flux across the outflow boundary Γ_{out} , which is defined as

$$(22) \quad Q = \frac{1}{|\Gamma_{\text{out}}|} \int_{\Gamma_{\text{out}}} \mathbf{q}(\cdot, \omega) \cdot \mathbf{n} \, dS,$$

where \mathbf{n} represents the outward unit vector normal to $\Gamma_{\text{out}} \subset \partial D$.

Our goal is to estimate the posterior mean of Q , defined as

$$(23) \quad \mathbb{E}_\nu[Q] = \int_\Omega Q(u) \, d\nu(u|p_{\text{obs}}),$$

by sampling the posterior distribution (21) using multilevel MCMC. As a reference to the reader, notation introduced and frequently used in this section is provided in Table 3.

TABLE 3. Bayesian inference notation.

Infinite-Dimensional Variable	Description
$d\mu(u)$	Prior density of u
p_{obs}	Observed local pressure data in D
$\pi^{\text{like}}(p_{\text{obs}} u)$	Likelihood function
$\nu(u p_{\text{obs}})$	Posterior density
$\mathbb{E}_{\nu}[\cdot]$	Mean with respect to posterior density
$Q = Q(u)$	Quantity of interest
Finite-Dimensional Variable	
$d\mu_{\ell}(u_{\ell})$	Prior density of u_{ℓ} on level ℓ
$\pi_{\ell}^{\text{like}}(p_{\text{obs}} u_{\ell})$	Likelihood function
$\nu_{\ell}(u_{\ell} p_{\text{obs}})$	Posterior density on level ℓ
α_{ℓ}^{SL}	Single-level acceptance probability on level ℓ
α_{ℓ}^{ML}	Multilevel acceptance probability on level ℓ
$\mathbb{E}_{\nu_{\ell}}[\cdot]$	Mean with respect to level ℓ posterior density
$\mathbb{V}_{\nu_{\ell}}[\cdot]$	Variance with respect to level ℓ posterior density
$Q_{\ell} = Q(u_{\ell})$	Quantity of interest on level ℓ

6.1. Markov Chain Monte Carlo. For the single-level approach, the log-permeability u , associated likelihood $\pi^{\text{like}}(p_{\text{obs}}|u)$, and QoI Q (see (5), (20), (22), and, respectively) are approximated numerically by solving the mixed PDEs in (5) and (18) utilizing a finite element approach on triangulation \mathcal{T}_k (for the finest level k). We denote these discrete approximations as u_k , π_k^{like} , and $Q_k = Q(u_k)$.

MCMC, and in particular, Metropolis-Hastings, is a modified Monte Carlo approach, where samples Q_k are generated from the target (posterior) distribution via a Markov chain. Then the posterior QoI expectation $\mathbb{E}_{\nu_k}[Q]$ may be approximated as

$$(24) \quad \hat{Q}_k^{MCMC} = \frac{1}{N} \sum_{i=n+1}^{n+N} Q_k^{(it)},$$

where $Q_k^{(it)} = Q(u_k^{(it)})$, n is the number of samples discarded as burn-in, and t is the subsampling rate to obtain independent samples (see Appendix A). To generate subsequent samples within a chain, a new u_k^{prop} is sampled from the proposal distribution and subjected to Metropolis-Hastings acceptance/rejection criterion. In this work, we utilize a preconditioned Crank-Nicolson stepping scheme with step size $\beta > 0$, where samples ψ_k from μ_k are drawn using Algorithm 4.2. Thanks to the prior-invariance of the preconditioned Crank-Nicolson proposal, the sample u_k^{prop} is then accepted with probability α_k^{SL} defined in (26) [20]. The procedure is summarized in Algorithm 6.1; additional details can be found in [27].

The cost of performing MCMC depends on how quickly the chain mixes as well as the variance of \hat{Q}_k . The first—the mixing of the chain—is controlled by the autocorrelation of samples within the chain. As adjacent samples in the chain are correlated (and not independent), the integrated autocorrelation time τ_Q of the chain will determine how many steps (and thus forward simulations) are required to get to the next independent sample. The second—the variance of \hat{Q}_k —is controlled by the number of independent samples used

Algorithm 6.1: Single level Metropolis-Hastings MCMC Algorithm with preconditioned Crank-Nicolson proposal to generate a posterior sample $u_k^{(i)} | u_k^{(i-1)}$

- Given $u_k^{(i-1)}$, propose u_k^{prop} using preconditioned Crank-Nicolson:

$$(25) \quad u_k^{\text{prop}} := \sqrt{1 - \beta^2} u_k^{(i-1)} + \beta \psi_k,$$

where $\psi_k \sim \mu_k$ is computed using Algorithm 4.2.

- Accept $u_k^{(i)} = u_k^{\text{prop}}$ with probability

$$(26) \quad \alpha_k^{SL}(u_k^{\text{prop}} | u_k^{(i-1)}) = \min \left\{ 1, \frac{\pi_k^{\text{like}}(p_{\text{obs}} | u_k^{\text{prop}})}{\pi_k^{\text{like}}(p_{\text{obs}} | u_k^{(i-1)})} \right\}$$

- Return $u_k^{(i)}$ and $Q_k^{(i)} = Q_k(u_k^{(i)})$.

in the estimator, i.e., N . The accuracy is similar to Monte Carlo in that the required number of (independent) samples to achieve a desired mean squared error depends on the variance of Q_k as well as the bias introduced by numerically approximating Q . If we require N independent simulations, with an integrated autocorrelation time (rounded up to an integer value) of t (see Appendix A), then we require at least tN simulations. Thus acceleration approaches should seek to reduce t and N by increasing the mixing of the chain and reducing the variance of the estimator, respectively.

6.2. Multilevel Markov Chain Monte Carlo. To accelerate MCMC, we consider the multilevel framework in [27], which utilizes chains at coarser spatial discretization levels to perform the majority of likelihood functions evaluations. Similar to previous sections, let us denote the log-normal permeability field, the Darcy pressure and flux, and the QoI at discretization level ℓ with the symbols u_ℓ , $(p_\ell, \mathbf{q}_\ell)$, $Q_\ell := Q_\ell(u_\ell)$, respectively, for $k = 0 \leq \ell \leq L$. Then the posterior mean of Q_0 is equivalently written as

$$(27) \quad \mathbb{E}_{\nu_0}[Q_0] = \mathbb{E}_{\nu_L}[Q_L] + \sum_{\ell=0}^{L-1} (\mathbb{E}_{\nu_\ell}[Q_\ell] - \mathbb{E}_{\nu_{\ell+1}}[Q_{\ell+1}]),$$

where ν_ℓ is the discrete posterior measure on level ℓ . Following [27], for each level ℓ , we define a multilevel estimator $\hat{Y}_\ell^{N_\ell}$ of the difference $\mathbb{E}_{\nu_\ell}[Q_\ell] - \mathbb{E}_{\nu_{\ell+1}}[Q_{\ell+1}]$ and write

$$(28) \quad \hat{Y}_\ell^{N_\ell} = \frac{1}{N_\ell} \sum_{i=n_\ell+1}^{n_\ell+N_\ell} Y_\ell^{(it_\ell)} = \frac{1}{N_\ell} \sum_{i=n_\ell+1}^{n_\ell+N_\ell} Q_\ell^{(it_\ell)} - Q_{\ell+1}^{(it_\ell t_{\ell+1})}.$$

Above n_ℓ corresponds to the burn-in on level ℓ , N_ℓ is the effective sample size on level ℓ (defined later in (31)), t_ℓ and $t_{\ell+1}$ are the estimated integrated autocorrelation times of the chains at levels ℓ and $\ell + 1$, respectively (see Appendix A for details). The key aspect of the multilevel MCMC is how to couple Markov chains at different levels so that: *i*) the variance of Y_ℓ is much smaller than that of Q_ℓ , *ii*) information from coarser level chains are used to accelerate mixing of finer level chains (higher acceptance rate, smaller integrated autocorrelation time). In this section, we focus on how to generalize the multilevel MCMC algorithm [27, Algorithm 3] to replace the KL decomposition-based sampling with our scalable multilevel PDE samplers described in Section 4.

As motivated in Remark 1, in what follow, we describe a two-level chain to evaluate the difference estimator \hat{Y}_ℓ at a generic level $0 \leq \ell < L$. Given a coarse sample $u_{\ell+1}^{(j-1)t_{\ell+1}}$, we advance the coarse chain at level $\ell + 1$ by $t_{\ell+1}$ steps using single-level Metropolis-Hastings as in Algorithm 6.1. This results in a coarse sample $u_{\ell+1}^{(jt_{\ell+1})}$ that is independent of $u_{\ell+1}^{(j-1)t_{\ell+1}}$.

To propose u_ℓ on the finer level ℓ , we use the two-level preconditioned Crank-Nicolson in (29), where ψ_ℓ is sampled from the conditional distribution $\psi_\ell | u_{\ell+1}^{(j-1)t_{\ell+1}}$ using Algorithm 4.3. Note that, the independence of $u_{\ell+1}^{(jt_{\ell+1})}$ from $u_{\ell+1}^{(j-1)t_{\ell+1}}$ guarantees that also ψ_ℓ is independent of $u_\ell^{(j-1)}$. That means that the two-level preconditioned Crank-Nicolson proposal in (29) satisfies the assumptions of [27, Lemma 3.1], and therefore the multilevel acceptance probability $\alpha_\ell^{ML}(u_\ell^{\text{prop}} | u_\ell^{(i-1)})$ in (30) satisfies the detailed balance condition. Algorithm 6.2 summarizes the generation of the paired fine and coarse level samples $u_\ell^{(j)}$ and $u_{\ell+1}^{(jt_{\ell+1})}$.

Note that, if u_ℓ^{prop} is accepted at step j , then $u_\ell^{(j)}$ and $u_{\ell+1}^{(jt_{\ell+1})}$ are correlated. Specifically, both $u_\ell^{(j)}$ and $u_{\ell+1}^{(jt_{\ell+1})}$ are generated from the same coarse level white noise functional $b_{\ell+1}$, and thus the difference $u_\ell^{(j)} - P_\ell u_{\ell+1}^{(jt_{\ell+1})}$ is small. This is observed in Section 4.1, where Figure 1 (b)-(c) display these differences, defined as solutions $u_0^{C\ell}$ (see (17)). This means that one should expect $Y_\ell^{(j)}$ to be small when step j is accepted, which is a necessary condition to achieve multilevel acceleration. The numerical results presented next indeed demonstrate that our algorithm is indeed able to achieve multilevel acceleration of the chain mixing and variance reduction.

Algorithm 6.2: Two-level Metropolis-Hastings MCMC Algorithm to generate paired samples $u_{\ell+1}^{(jt_{\ell+1})}$ and $u_\ell^{(j)} | u_\ell^{(j-1)}$

Part I. Advance the coarse chain at level $\ell + 1$ by $t_{\ell+1}$ steps:

- Given $u_{\ell+1}^{(j-1)t_{\ell+1}}$, apply Algorithm 6.1 on level $\ell + 1$ for $t_{\ell+1}$ steps
- Store $u_{\ell+1}^{(jt_{\ell+1})}$ and $Q(u_{\ell+1}^{(jt_{\ell+1})})$

Part II. Advance the fine chain at level ℓ by one step:

- Given $u_\ell^{(j-1)}$ and $u_{\ell+1}^{(jt_{\ell+1})}$, propose u_ℓ^{prop} :

$$(29) \quad u_\ell^{\text{prop}} := \sqrt{1 - \beta^2} u_\ell^{(j-1)} + \beta \psi_\ell,$$

where $\psi_\ell | u_{\ell+1}^{(jt_{\ell+1})}$ is sampled using Algorithm 4.3.

- Accept $u_\ell^{(j)} = u_\ell^{\text{prop}}$ with probability

$$(30) \quad \alpha_\ell^{ML}(u_\ell^{\text{prop}} | u_\ell^{(i-1)}) = \min \left\{ 1, \frac{\pi_\ell^{\text{like}}(p_{\text{obs}} | u_\ell^{\text{prop}}) \pi_{\ell+1}^{\text{like}}(p_{\text{obs}} | u_{\ell+1}^{(j-1)t_{\ell+1}})}{\pi_\ell^{\text{like}}(p_{\text{obs}} | u_\ell^{(j-1)}) \pi_{\ell+1}^{\text{like}}(p_{\text{obs}} | u_{\ell+1}^{(jt_{\ell+1})})} \right\}.$$

- Return $u_\ell^{(j)}$, $u_{\ell+1}^{(jt_{\ell+1})}$, $Y_\ell^{(j)} = Q(u_\ell^{(j)}) - Q(u_{\ell+1}^{(jt_{\ell+1})})$

Remark 1. Another small difference with respect to the work in [27] is that each $\hat{Y}_\ell^{N_\ell}$ estimate uses only two levels. Specifically, Algorithm 6.2 uses a single auxiliary chain on the coarser level $\ell + 1$ to estimate \hat{Y}_ℓ , while [27] runs auxiliary chains on all coarser levels. Our decision to do this is based on algorithmic simplicity and scalability. That said, utilizing all coarser levels is a detail that may be considered in future work.

TABLE 4. Time in seconds to generate 50 Gaussian random field realizations using (16). Runs were completed on LLNL Quartz.

Level ℓ	Number Elements	NP=2	NP =4	NP =8	NP =16	NP =32	NP = 64
0	196,608	308	161	75.2	42.9	23.2	12.0
1	24,576	27.9	10.9	5.87	3.88	2.94	2.55
2	3,072	2.18	1.49	1.11	1.03	1.07	1.18

6.3. Three-Level Markov Chain Monte Carlo Results. To demonstrate our method, we consider a three-level MCMC with the hierarchical stochastic PDE solver by utilizing Algorithm 6.2. The computational domain is a unit cube discretized with tetrahedral elements. For the prior, we consider Gaussian random fields with correlation length $\lambda = 0.3$ and marginal variance of $\sigma^2 = 0.5$. Table 4 provides information regarding the number of elements in each level, as well as the wall time needed to generate 50 realizations of u_k for various numbers of processors. While we may consider a level dependent number of processors based on these scaling results (which is a possible future direction), in the following computations we fix the total number of processors to 8. For the observational pressure data, we synthetically generate a realization p_{obs} with $\sigma_\eta^2 = 0.005$; this is done via (19) on a reference mesh with approximately 12.5M elements.

For each $\hat{Y}_\ell^{N_\ell}$ ($\ell = 0, 1$) estimate, we run a single chain using step size $\beta^2 = 0.3$ on each level. First we investigate the subsampling rate we require for Y_0 and Y_1 components in order to obtain independent samples. To do so, we run a chain using the multilevel MCMC approach in Algorithm 6.2 with 2,000 fine level burn-in samples, and a running estimate of the integrated autocorrelation time (see Appendix A for details). Figure 4 displays the autocorrelation of the different level chains (from a single run) as a function of the lag time, after performing an additional 2,000 effective samples on the fine level. Figure 4 (a) compares the decay in autocorrelation for the coarse level chain QoI Q_2 with the fine level chain QoI (as formed via the hierarchical approach) $Y_1 = Q_1 - Q_2$, while Figure 4 (b) compares that of Q_1 and $Y_0 = Q_0 - Q_1$. Faster decays indicate faster mixing of the chain, as fewer steps in the chain result in an uncorrelated sample. From these two results, performing the hierarchical multilevel estimates of Y_ℓ improve the fine level mixing.

Once the chain is completed, the average maximum integrated autocorrelation times are estimated for each level. The coarse level chain of Q_2 values has an approximate integrated autocorrelation time of 58, and the correction terms have integrated autocorrelation times of 5 for $Y_1 = Q_1 - Q_2$ and 4 for $Y_0 = Q_0 - Q_1$. The drastic reduction in integrated autocorrelation time demonstrates the effectiveness of the two-level MCMC in accelerating mixing.

In addition to estimating the integrated autocorrelation time, we investigate the improvement in the acceptance rate on the finer levels. Figure 5 (a) displays the average acceptance rate from the three chains, on the three different levels. With a fixed $\beta^2 = 0.3$ (for both levels), the acceptance rate of the coarse level $\ell = 2$ is about 0.33, while that of level $\ell = 1$ is 0.68, and that of level 0 is 0.83. This increase in the accepted rate is similar to that reported in [27], numerically demonstrating that indeed our method using multilevel stochastic PDE samplers is a computationally efficient alternative to KL-decomposition based sampling for multilevel MCMC.

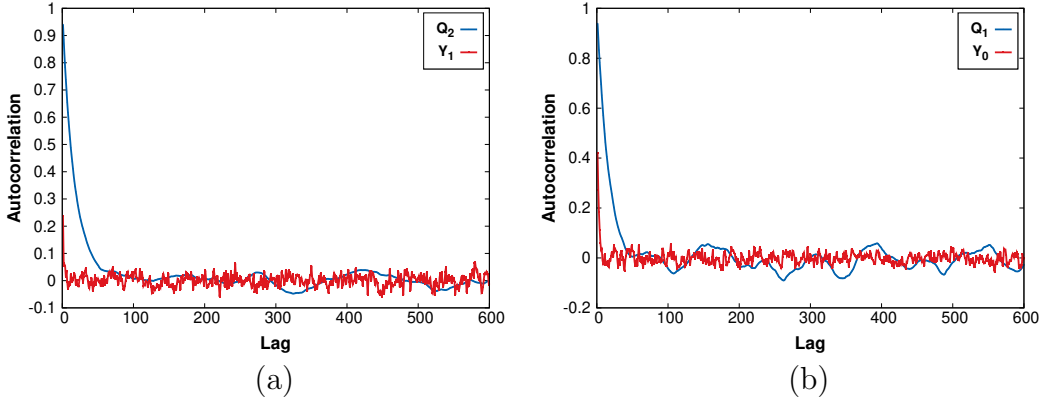


FIGURE 4. Autocorrelation estimates for increasing lag time, which will be used to estimate the subsampling rate t_ℓ for $\ell = 0, 1, 2$. (a) Comparison of the autocorrelation estimate of Q_2 simulations and $Y_1 = Q_1 - Q_2$ simulations. (b) Comparison of the autocorrelation estimate of Q_1 simulations and $Y_0 = Q_0 - Q_1$ simulations.

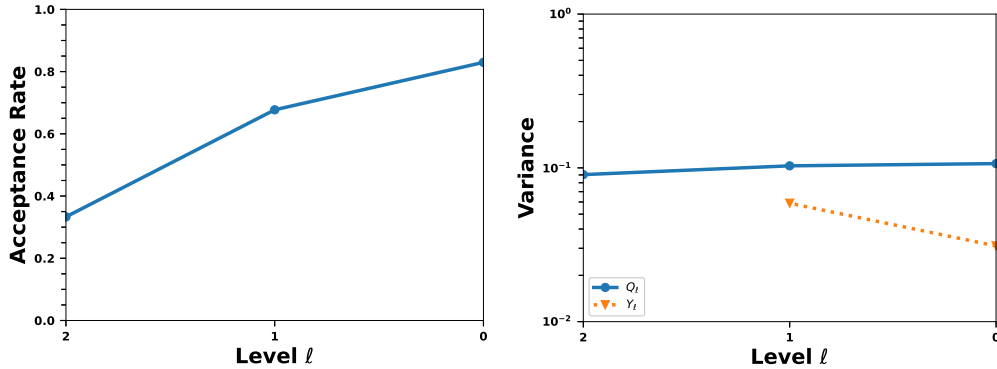


FIGURE 5. (a) Increase in acceptance rate moving from coarse to fine level, indicating improved mixing on the finer levels. (b) Variance estimates for Q_ℓ and $Y_\ell = Q_\ell - Q_{\ell+1}$. The decay in the variance estimate of Y_ℓ (for decreasing ℓ) is essential for multilevel MCMC to be more cost efficient than the single-level approach.

Next, we consider the estimated variance of the Y_ℓ for levels $\ell = 0, 1, 2$. Figure 5 (b) provides variance estimates for Q_ℓ on each level, as well as variance estimates for the correction terms $Y_\ell = Q_\ell - Q_{\ell+1}$. The decay in the Y_ℓ variance estimate indicates that fewer samples will be required on the finest levels (relative to the coarsest) for a specified error bound. This result is similar to that of [27]; however, our decay is not quite as rapid – this is likely due to the difference in our problem setup ($d = 3$, $\lambda = 0.3$), as well as the fact that we’re doing inference in a higher-dimensional space. More specifically, we have one DOF per element with 196K elements on the finest level, while the work in [27] has a KL expansion truncated at 150 DOFs on the finest level.

The final result we consider is the total computational cost of this multilevel approach. To determine the total number of samples required in the level ℓ chain of Algorithm 6.2, we

utilize the approach in [27], where

$$(31) \quad N_\ell^{\text{eff}} = \frac{2}{\varepsilon^2} \left(\sum_{k=0}^L \sqrt{\mathbb{V}_{\nu_k, \nu_{k+1}}[Y_k] \mathcal{C}_k^{\text{eff}}} \right) \sqrt{\frac{\mathbb{V}_{\nu_\ell, \nu_{\ell+1}}[Y_\ell]}{\mathcal{C}_\ell^{\text{eff}}}}$$

is the total number of effective samples to estimate the expectation, with variance $\mathbb{V}_{\nu_\ell, \nu_{\ell+1}}[Y_\ell]$ (with respect to the joint distribution of u_ℓ and $u_{\ell+1}$) and effective cost per independent sample of Y_ℓ defined as

$$(32) \quad \mathcal{C}_\ell^{\text{eff}} := t_\ell(\mathcal{C}_\ell + t_{\ell+1}\mathcal{C}_{\ell+1});$$

here \mathcal{C}_ℓ is the cost to calculate a single simulation of Q_ℓ . With an estimated integrated autocorrelation time of t_ℓ , we require $N_\ell^{\text{total}} = t_\ell N_\ell^{\text{eff}}$ samples of Y_ℓ . We note, this does not include the total number of samples discarded for the burn-in. In [27], the authors discard the first $n_\ell = 2t_\ell$ samples as burn-in. Using the prior results regarding integrated autocorrelation time, variance estimates, and simulation time for $NP = 8$, we estimate that performing a three-level MCMC is 58% the cost of performing a single-level MCMC.

6.4. Discussion. The novelty and advantages of our two-level preconditioned Crank-Nicholson proposal in Algorithm 6.2 lies in the use of a scalable, memory efficient stochastic PDE sampler in lieu of a computationally and memory expensive KL-decomposition. However, our method shares the same structure and benefits of the original KL-based approach in [27]. In fact, both proposals are linear transformations of independent Gaussian vectors defined on the coarse and fine grids: the coarser-level random variables define the smooth components of the random field u_ℓ , while the finer-level random variables control the high frequency components of u_ℓ . The only—but key—difference is in how the transformation is defined. Our method uses sparse finite element interpolation operators and scalable fast PDE linear solvers; the one in [27] uses dense matrices whose columns represents the dominant eigenvectors of the covariance method. As our numerical result showed, Algorithm 6.2 offers comparable multilevel acceleration to that presented in [27]. First, the great majority of likelihood evaluations are done the coarse levels of the hierarchy, where evaluating the forward model is inexpensive. Second, the acceptance rate improves as the mesh is refined thus reducing the variance of the estimator \hat{Y}_ℓ at finer levels. Third, the auxiliary coarse level chain allows for drastically reducing the integrated autocorrelation time t_ℓ thanks to the use of independent samples from the coarse chain. We argue that the increase of the acceptance rate is due to the smoothing properties of the forward map in (19). A characteristic feature of inverse problems governed by PDEs is that the smooth components of the parameter are the most informed by the data, while the likelihood function is not very sensitive to perturbations in highly oscillatory components of u . This can be proven analytically for certain linear forward PDE problems (e.g. advection-diffusion [31], Poisson [32], Stokes [58], acoustics [12, 13], electromagnetics [14]), and demonstrated numerically for more complex PDE problems (e.g. seismic wave propagation [15, 11], mantle convection [59], ice sheet flow [42, 51], poroelasticity [39], and turbulent flow [17]). As numerically illustrated in Section 4.1, our hierarchical sampler induces a multiscale decomposition of the random field u , where finer-level proposal u_ℓ shares the same smooth components of the corresponding sample from the posterior distribution $\nu_{\ell+1}$ at the coarser-level $\ell + 1$. As we move to finer and finer levels we expect the likelihood function to become insensitive to the difference $u_\ell - Pu_{\ell+1}$, thus drastically increasing the acceptance rate. The increased mixing of the chain is then a direct

consequence of the increased acceptance rate and of the independence of the coarse grid samples used in the two-level preconditioned Crank-Nicholson proposal.

7. CONCLUSION

In this work we develop a new hierarchical approach to generate Gaussian random field realizations that will scale with the refinement of the discretization, and thus is well apt for large-scale three-dimensional simulations. Building off of approaches from [49, 50], we extend the work into a hierarchical multilevel framework by performing a hierarchical decomposition of white noise across multiple levels of discretization. From this hierarchical decomposition, we may generate corresponding realizations of discrete Gaussian random fields, such that fine scale random fields are generated in a hierarchical fashion from coarse scale random fields. The key result of this decomposition is that it allows for independent MCMC stepping across the different levels of discretization without forming a KL-based hierarchy.

The theoretical results of this paper prove that this hierarchical approach does in fact generate Gaussian random fields on each level, and numerical results show that, when utilizing scalable solvers, this approach is scalable. The particular solvers that we use in this approach are shown to provide fine level scalability. A current drawback of this implementation is that the coarser levels do not scale as well. This is due to the number of processors; in particular, the fine level scales in a different regime than the coarse levels, and thus we see decreased efficiency on the coarser levels, as shown in the numerical results. To improve this issue, one approach would be to utilize the framework of [28], where they distribute the work across a number of processors that is level dependent.

Possible future directions of this work include performing this multilevel MCMC approach with a more informed proposal, e.g., local Hessian information, as in [23, 22]. In particular, [22] combines the multilevel approach of [27] with dimension-independent likelihood-informed MCMC samplers of [23] to further accelerate multilevel MCMC.

APPENDIX A. INTEGRATED AUTOCORRELATION TIME

To obtain independent samples for unbiased estimates of QoI moments from the chain $\{Q_0^{(i)}\}_{i>0}$, we subsample the chain according to its integrated autocorrelation time τ_Q . In this work, we estimate τ_Q as

$$(33) \quad \hat{\tau}_Q = 1 + 2 \sum_{\tau=1}^M \hat{\rho}_Q(\tau)$$

where the normalized autocorrelation function is estimated as

$$(34) \quad \hat{\rho}_Q(\tau) = \frac{1}{N - \tau} \sum_{i=1}^{N-\tau} \frac{(Q_0^{(i)} - \hat{\mu}_Q)(Q_0^{(i+\tau)} - \hat{\mu}_Q)}{\hat{\sigma}_Q^2},$$

with $\hat{\mu}_Q$ and $\hat{\sigma}_Q^2$ as the estimated mean and variance (respectively) of the data $\{Q_0^{(i)}\}_{i=1}^N$, and $M \ll N$ (see [54] for more information on integrated autocorrelation time).

In practice we subsample at a rate of $t := \lceil \hat{\tau}_Q \rceil$. We denote t_ℓ (with $\ell < L$) as the estimate for the multilevel chains $\{Y_\ell^{(i)}\}_{i>0}$.

REFERENCES

- [1] GLVis: Opendgl finite element visualization tool. glvis.org.
- [2] HYPRE: High performance preconditioners. <http://www.llnl.gov/CASC/hypre/>.
- [3] MFEM: Modular finite element methods library. mfem.org.
- [4] ParELAG: Element-agglomeration algebraic multigrid and upscaling library, version 2.0. <http://github.com/LLNL/parelag>, 2015.
- [5] ParELAGMC: Parallel element agglomeration multilevel Monte Carlo library. <http://github.com/LLNL/parelagmc>, 2018.
- [6] R.J. Adler and J.E. Taylor. *Random fields and geometry*. Springer Science & Business Media, 2009.
- [7] R.J. Adler, J.E. Taylor, and K.J. Worsley. Applications of random fields and geometry: foundations and case studies. 2007. In preparation.
- [8] A. Barth, C. Schwab, and N. Zollinger. Multi-level Monte Carlo finite element method for elliptic PDEs with stochastic coefficients. *Numerische Mathematik*, 119(1):123–161, 2011.
- [9] M. Bebendorf. *Hierarchical matrices*. Springer, 2008.
- [10] A. Beskos, M. Girolami, S. Lan, P.E. Farrell, and A.M. Stuart. Geometric MCMC for infinite-dimensional inverse problems. *Journal of Computational Physics*, 335:327–351, 2017.
- [11] T. Bui-Thanh, C. Burstedde, O. Ghattas, J. Martin, G. Stadler, and L.C. Wilcox. Extreme-scale UQ for Bayesian inverse problems governed by PDEs. In *Proceedings of the International Conference on High Performance Computing, Networking, Storage and Analysis*, page 3. IEEE Computer Society Press, 2012.
- [12] T. Bui-Thanh and O. Ghattas. Analysis of the Hessian for inverse scattering problems. Part II: Inverse medium scattering of acoustic waves. *Inverse Problems*, 28(5):055002, 2012.
- [13] T. Bui-Thanh and O. Ghattas. Analysis of the Hessian for inverse scattering problems. Part III: Inverse medium scattering of electromagnetic waves. *Inverse Problems and Imaging*, 7(4):1139–1155, 2013.
- [14] T. Bui-Thanh and O. Ghattas. Randomized maximum likelihood sampling for large-scale Bayesian inverse problems. *In preparation*, 2013.
- [15] T. Bui-Thanh, O. Ghattas, J. Martin, and G. Stadler. A computational framework for infinite-dimensional Bayesian inverse problems part I: The linearized case, with application to global seismic inversion. *SIAM Journal on Scientific Computing*, 35(6):A2494–A2523, 2013.
- [16] T. Bui-Thanh and M.A. Girolami. Solving large-scale PDE-constrained Bayesian inverse problems with Riemann manifold Hamiltonian Monte Carlo. *Inverse Problems*, 30:114014, 2014.
- [17] P. Chen, U. Villa, and O. Ghattas. Taylor approximation and variance reduction for PDE-constrained optimal control under uncertainty. *Journal of Computational Physics*, 385:163–186, 2019.
- [18] J.A. Christen and C. Fox. Markov chain Monte Carlo using an approximation. *Journal of Computational and Graphical Statistics*, 14(4):795–810, 2005.
- [19] K.A. Cliffe, M.B. Giles, R. Scheichl, and A.L. Teckentrup. Multilevel Monte Carlo methods and applications to elliptic PDEs with random coefficients. *Computing and Visualization in Science*, 14(1):3–15, 2011.
- [20] S.L. Cotter, G.O. Roberts, A.M. Stuart, and D. White. MCMC methods for functions: modifying old algorithms to make them faster. *Statistical Science*, pages 424–446, 2013.
- [21] M. Croci, M.B. Giles, M.E. Rognes, and P.E. Farrell. Efficient white noise sampling and coupling for multilevel Monte Carlo with nonnested meshes. *SIAM/ASA Journal on Uncertainty Quantification*, 6(4):1630–1655, 2018.
- [22] T. Cui, G. Detommaso, and R. Scheichl. Multilevel dimension-independent likelihood-informed mcmc for large-scale inverse problems. *arXiv preprint arXiv:1910.12431*, 2019.
- [23] T. Cui, K.J.H. Law, and Y.M. Marzouk. Dimension-independent likelihood-informed MCMC. *Journal of Computational Physics*, 304:109–137, 2016.
- [24] T. Cui, J. Martin, Y.M. Marzouk, A. Solonen, and A. Spantini. Likelihood-informed dimension reduction for nonlinear inverse problems. *Inverse Problems*, 30(11):114015, 2014.
- [25] Y. Daon and G. Stadler. Mitigating the influence of the boundary on PDE-based covariance operators. *Inverse Problems & Imaging*, 12(5):1083–1102, 2018.

- [26] V. Dobrev, T. Kolev, C.S. Lee, V. Tomov, and P.S. Vassilevski. Algebraic hybridization and static condensation with application to scalable $\mathbf{H}(\text{div})$ preconditioning. *SIAM Journal on Scientific Computing*, 41(3):B425–B447, 2019.
- [27] T.J. Dodwell, C. Ketelsen, R. Scheichl, and A.L. Teckentrup. A hierarchical multilevel Markov chain Monte Carlo algorithm with applications to uncertainty quantification in subsurface flow. *SIAM/ASA Journal on Uncertainty Quantification*, 3(1):1075–1108, 2015.
- [28] D. Drzisga, B. Gmeiner, U. Rüde, R. Scheichl, and B. Wohlmuth. Scheduling massively parallel multigrid for multilevel Monte Carlo methods. *SIAM Journal on Scientific Computing*, 39(5):S873–S897, 2017.
- [29] Y. Efendiev, T. Hou, and W. Luo. Preconditioning Markov chain Monte Carlo simulations using coarse-scale models. *SIAM Journal on Scientific Computing*, 28(2):776–803, 2006.
- [30] Y. Efendiev, B. Jin, P. Michael, and X. Tan. Multilevel Markov chain Monte Carlo method for high-contrast single-phase flow problems. *Communications in Computational Physics*, 17(1):259–286, 2015.
- [31] H.P. Flath, L.C. Wilcox, V. Akcelik, J. Hill, B. van Bloemen Waanders, and O. Ghattas. Fast algorithms for Bayesian uncertainty quantification in large-scale linear inverse problems based on low-rank partial hessian approximations. *SIAM Journal on Scientific Computing*, 33(1):407–432, 2011.
- [32] P.H. Flath. *Hessian-based response surface approximations for uncertainty quantification in large-scale statistical inverse problems, with applications to groundwater flow*. PhD thesis, The University of Texas at Austin, 2013.
- [33] R.G. Ghanem and P.D. Spanos. *Stochastic finite elements: a spectral approach*. Courier Corporation, 2003.
- [34] M.B. Giles. Multilevel Monte Carlo path simulation. *Operations Research*, 56(3):607–617, 2008.
- [35] C.J. Gittelsohn, J. Könnö, C. Schwab, and R. Stenberg. The multi-level Monte Carlo finite element method for a stochastic Brinkman problem. *Numerische Mathematik*, 125(2):347–386, 2013.
- [36] I.G. Graham, F.Y. Kuo, D. Nuyens, R. Scheichl, and I.H. Sloan. Analysis of circulant embedding methods for sampling stationary random fields. *SIAM Journal on Numerical Analysis*, 56(3):1871–1895, 2018.
- [37] W.K. Hastings. Monte Carlo sampling methods using Markov chains and their applications. 1970.
- [38] S. Heinrich. Multilevel Monte Carlo methods. In *Large-scale scientific computing*, pages 58–67. Springer, 2001.
- [39] M. Hesse and G. Stadler. Joint inversion in coupled quasistatic poroelasticity. *Journal of Geophysical Research: Solid Earth*, 119(2):1425–1445, 2014.
- [40] D. Higdon, H. Lee, and Z. Bi. A Bayesian approach to characterizing uncertainty in inverse problems using coarse and fine-scale information. *IEEE Transactions on Signal Processing*, 50(2):389–399, 2002.
- [41] V.H. Hoang, J.H. Quek, and C. Schwab. Analysis of multilevel MCMC-FEM for Bayesian inversion of log-normal diffusions. *Inverse Problems*, 2019.
- [42] T. Isaac, N. Petra, G. Stadler, and O. Ghattas. Scalable and efficient algorithms for the propagation of uncertainty from data through inference to prediction for large-scale problems, with application to flow of the antarctic ice sheet. *Journal of Computational Physics*, 296:348–368, 2015.
- [43] J.D. Jansen, R.M. Fonseca, S. Kahrobaei, M.M. Siraj, G.M. Van Essen, and P.M.J. Van den Hof. The egg model—a geological ensemble for reservoir simulation. *Geoscience Data Journal*, 1(2):192–195, 2014.
- [44] U. Khristenko, L. Scarabosio, P. Swierczynski, E. Ullmann, and B. Wohlmuth. Analysis of boundary effects on PDE-based sampling of Whittle–Matérn random fields. *SIAM/ASA Journal on Uncertainty Quantification*, 7(3):948–974, 2019.
- [45] C.S. Lee and P.S. Vassilevski. Parallel solver for $\mathbf{H}(\text{div})$ problems using hybridization and AMG. In *Domain Decomposition Methods in Science and Engineering XXIII*, pages 69–80. Springer, 2017.
- [46] F. Lindgren, H. Rue, and J. Lindström. An explicit link between Gaussian fields and Gaussian Markov random fields: the stochastic partial differential equation approach. *Journal of the Royal Statistical Society: Series B (Statistical Methodology)*, 73(4):423–498, 2011.
- [47] J. Martin, L.C. Wilcox, C. Burstedde, and O. Ghattas. A stochastic Newton MCMC method for large-scale statistical inverse problems with application to seismic inversion. *SIAM Journal on Scientific Computing*, 34(3):A1460–A1487, 2012.
- [48] N. Metropolis, A.W. Rosenbluth, M.N. Rosenbluth, A.H. Teller, and E. Teller. Equation of state calculations by fast computing machines. *The journal of chemical physics*, 21(6):1087–1092, 1953.

- [49] S. Osborn, P.S. Vassilevski, and U. Villa. A multilevel, hierarchical sampling technique for spatially correlated random fields. *SIAM J. Sci. Comput.*, 39(5):S543–S562, 2017.
- [50] S. Osborn, P. Zulian, T. Benson, U. Villa, R. Krause, and P.S. Vassilevski. Scalable hierarchical PDE sampler for generating spatially correlated random fields using nonmatching meshes. *Numerical Linear Algebra with Applications*, 25(3):e2146, 2018.
- [51] N. Petra, J. Martin, G. Stadler, and O. Ghattas. A computational framework for infinite-dimensional Bayesian inverse problems, part II: Stochastic Newton MCMC with application to ice sheet flow inverse problems. *SIAM Journal on Scientific Computing*, 36(4):A1525–A1555, 2014.
- [52] C. Robert and G. Casella. *Monte Carlo statistical methods*. Springer Science & Business Media, 2013.
- [53] L. Roininen, J.M.J. Huttunen, and S. Lasanen. Whittle-Matérn priors for bayesian statistical inversion with applications in electrical impedance tomography. *Inverse Problems & Imaging*, 8(2):561, 2014.
- [54] A. Sokal. Monte Carlo methods in statistical mechanics: foundations and new algorithms. In *Functional integration*, pages 131–192. Springer, 1997.
- [55] A.M. Stuart. Inverse problems: a Bayesian perspective. *Acta numerica*, 19:451–559, 2010.
- [56] A.L. Teckentrup, R. Scheichl, M.B. Giles, and E. Ullmann. Further analysis of multilevel Monte Carlo methods for elliptic PDEs with random coefficients. *Numerische Mathematik*, 125(3):569–600, 2013.
- [57] P. Whittle. Stochastic processes in several dimensions. *B. Int. Statist. Inst.*, 40:974–994, 1963.
- [58] J. Worthen. *Inverse Problems in Mantle Convection: Models, Algorithms, and Applications*. PhD thesis, The University of Texas at Austin, 2012.
- [59] J. Worthen, G. Stadler, N. Petra, M. Gurnis, and O. Ghattas. Towards adjoint-based inversion for rheological parameters in nonlinear viscous mantle flow. *Physics of the Earth and Planetary Interiors*, 234:23–34, 2014.